

SOUR CORROSION OF API 5L X70 MO CARBON STEELS IN NACE TM 0177B SOLUTION

Élida Mariana Almeida Alves¹, Giovanna Campos Fernandes¹, Pietra Alice Marcelino Soares², Pedro Martorelli Pinheiro ¹, Sandro Martins Ribeiro¹, Rafael Lucas Resende¹, Rosinei Batista Ribeiro², Elioenai Levi Barbedo³, Heloisa Andréa Acciari¹, Eduardo Norberto Codaro¹

e-mail: elida.alves@unesp.br

¹Unesp - Campus de Guaratinguetá, Av. Dr. Ariberto Pereira da Cunha, 333, Portal das Colinas, CEP 12516-410, Guaratinguetá - SP

²CEETEPS – UPEP - FATEC- Guaratinguetá, Av. Prof. João Rodrigues Alckmin, 1.501, Jardim Esperança, CEP 12517-475, Guaratinguetá - SP.

³Unifei- Campus Prof. José Rodrigues Seabra, Av. B P S, 1303 - Pinheirinho, Itajubá - MG, 37500-903

Abstract:

AISI 5L X70 steels are used in pipelines, where their purpose is to contribute to the microstructural understanding of corrosion causes and mechanisms. This study aims to investigate the factors influencing corrosion mechanisms in AISI 5L X70 MO and MS steels. The methodological steps adopted for the development of this work included: preparation of specimens for microstructural characterization; immersion in NACE 177-B solution, subjected to deaerated steam for 12 hours and saturated with H₂S for 96 hours under steam from this solution at room temperature; analysis of corrosion products by scanning electron microscopy, EDS, and X-ray diffractometry. The as-received sample was attacked with 2% Nital solution for 7 seconds, with predominantly ferrite and pearlite microstructure. The MS revealed a ferritic matrix and intergranular ferritic aspects, while X70 MO has a ferritic microstructure with banding caused by microsegregation of alloying elements during the manufacturing process. Grain size was determined as 6 μm ± 3 for MO and 5 μm ± 2 for MS. Evaluating grain size, the microhardness HV with a load of 0.1 Kgf/mm² for the steels, the average and standard deviation for MO in the banded region were 221.32 HV ± 22.63, and outside the banding region was 217.04 HV ± 21.14; for MS, it was 227.77 HV ± 7.60. Corrosion resistance of specimens was assessed by mass loss. MO samples exhibited higher resistance to the environment without H₂S compared to MS. Scanning electron microscopy and EDS in secondary electron mode

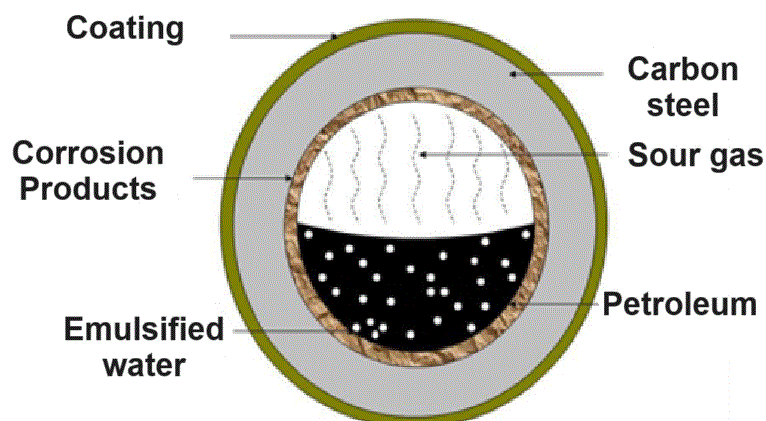
revealed a homogeneous microstructure related to grain size and the presence of sulfur and manganese, likely nucleated by the inclusion of MnS. Comparative mass loss results indicated that MO demonstrated greater corrosion resistance due to its higher homogeneity and microstructure refinement, however, MS exhibited banding characteristics, leading to the formation of MnS inclusions.

Keywords: API 5L X70, Pipeline, Microstructural, Corrosion.

Introduction

In recent decades, the world has seen continuous growth in demand for oil and natural gas. Despite all efforts to diversify the world's energy matrix, current projections still indicate an increase in demand for these fluids in the coming decades. This demand, combined with the desire of many nations to obtain strategic autonomy in relation to their energy matrices, has led to an increase in prospecting and exploration operations for increasingly complex deposits. These deposits present greater geological and geographical difficulties, as well as “sourer” oil [1]. During primary recovery, the fluid that spontaneously leaves the wells of a deposit goes through a process in which the crude oil, natural gas and formation water are separated. After primary processing, the stabilized oil is pumped to the port terminals and then to the refineries, arriving there with a vapor pressure of less than 0.7 atm at room temperature. Hydrogen sulfide, which naturally does not contain oil, together with emulsified water and water vapor, becomes an environmental acid suitable for corrosion, known as acid [2-4] (Figure 1).

Figure 1: Illustration of the cross section of an oil pipeline showing the scale formed by sour corrosion



In this environment, transfer pipes and storage tanks, commonly made from carbon steel, can suffer localized or even generalized corrosion, depending on the steel, oil and operational conditions such as pressure, temperature and flow dynamics [5,6]. Among the types of localized corrosion, the so-called hydrogen embrittlement stands out as the most worrying form of corrosion. In this process, part of the hydrogen that is reduced during the corrosion reaction penetrates the steel and accumulates in discontinuities and defects, which after certain pressurization lead to the formation of cracks and, finally, brittle fracture, since these materials are always subjected to external requests

Many professionals linked to oil companies dedicated themselves to studying the corrosive processes of carbon steels in the presence of sulfides and in this mission the analysis of corrosion products in pipelines was decisive in the retrospective study of the corrosion mechanism. The research problem was behavior experience combined with scientific research made it possible to discern, to a certain extent, which of those products were formed as a result of corrosion and which of oil contamination during production. The objective was to characterize the corrosion of API 5L X70 MS and MO steels in NACE 177-B solution saturated with H₂S and deaerated to identify corrosion products.

Experimental Procedure

The low carbon, high mechanical strength steels API 5L X70 MO and MS were supplied by a petrochemical company in South America. Samples were

taken from 22-inch pipes by plasma cutting at approximately 90 degrees of the longitudinal weld. API X70 MO steel has a higher carbon, phosphorus, sulfur manganese content and rolling prior to tube forming was conventional.

This steel was designed to withstand an onshore environment with low concentration of H₂S. The other API X70 MS steel was subjected to controlled rolling and accelerated cooling and designed to withstand a sour environment. Corrosion tests for 12 hours deaerated with nitrogen input were carried out on the device for the purpose of verifying the formation of a film the solution used was deaerated with a constant flow of N₂, before and during the test, at room temperature of 24°C shown in the Figure 1.

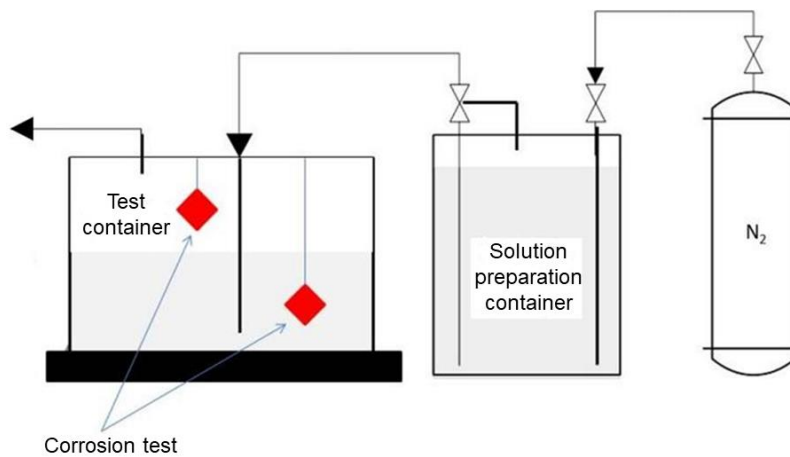
The 96-hour corrosion test was carried out in the steel supplying industry itself shown in the Figure 2. Subsequently, the chemical components that come into contact with the steel were studied in order to solve the previous problems by carrying out corrosion tests and chemical attacks. Both corrosion tests were carried out immersed and suspended in the NACE 177 B solution at room temperature.

The samples for test corrosion 12 and 96 hours (MO 20 x 25 mm and MS 20x20 mm) were sanded with #100, 220, 400 and 600 ~~mesh sandpaper~~, washed, dried and weighed on a semi-analytical balance. The NACE 177-B solution has the following composition: NaCl 5.0% + CH₃COOH 2.5% + CH₃COONa 0.41% by mass and pH ≈ 3.45.

The solution was deaerated with a constant flow of N₂, before and during the test, at room temperature. After the 12-hour and 96-hour tests, the samples were dried under vacuum and stored in the desiccator, to avoid contact with oxygen until the time to perform X-ray diffraction.

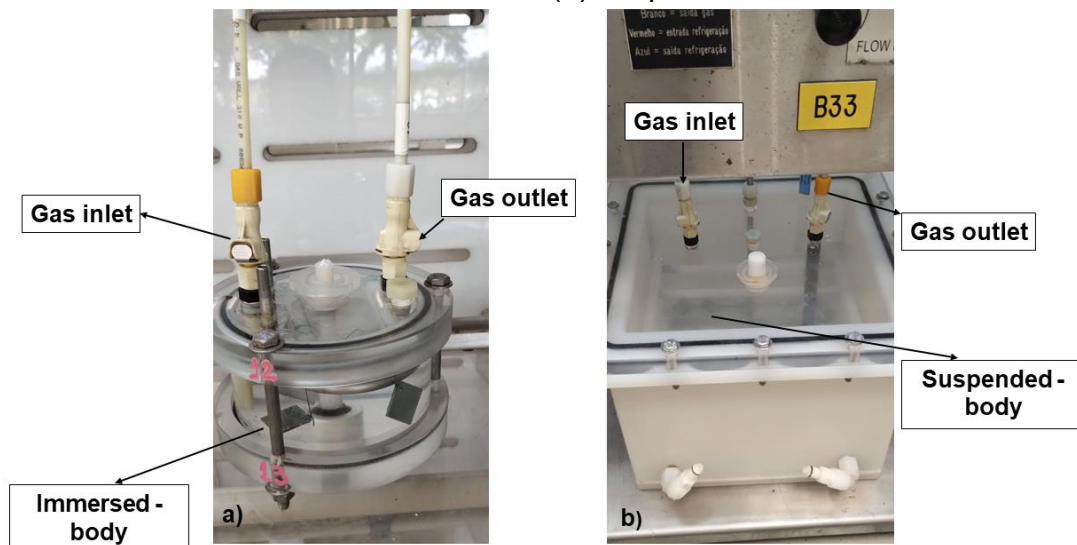
Next, the 12-hour and 96-hour samples were pickled with Clark's solution (50 g of SnCl₂ + 20 g Sb₂O₃ + 1 L of HCl_{conc}) at intervals of 5 min learning, dried, weighed and the relative mass loss percentage per unit (PMR%) was calculated using Eq. 1, with *m*_i and *m*_f being the initial and final mass of the samples and their exposed area (*A*).

Figure 2: Corrosion testing device used in work



$$\text{PMR}\% = \left[\frac{(m_i - m_f)}{(m_i \times A)} \right] \times 100 \quad (1)$$

Figure 3: Electrolytic Cell with devices used for corrosion tests 96 hours (a) immersion and (b) suspended.



Chemical composition of these samples in Table 1 was determined by optical emission spectrometry with a Terno Scientific ARL OES Spectrometer and 1 ACO-BL software.

Tabela 1: Chemical composition of API 5L X70MS and API 5L X 70MO steels (wt. %)

Steel	Chemical composition (Weight%)											
	C	S	Mn	P	Si	Al	Ni	Cr	Cu	Mo	Ti	Others
X70 MO	0,09	0,003	1,58	0,02	0,28	0,03	0,02	0,03	0,02	0,0039	0,02	a
X70 MS	0,03	0,002	1,29	0,02	0,28	0,02	0,17	0,17	0,16	0,05	0,01	b
a	V= 0,003 4%;	As= 0,01; %	Nb= 0,05 %;	N= 0,00 5%;	Bi= 0,00 2%;	Ca= 0,00 1%;	Co= 0,00 7%;	Zn= 0,001 %;	Sb= 0,00 2%;	Ta= 0,010 %;	W= 0,00 9%;	Pb= 0,001% %
b	V= 0,05 %;	As= 0,01 %;	Nb= 0,03 %;	N= 0,00 5%;	Bi= 0,00 2%;	Ca= 0,00 2%;	Co= 0,00 2%;	Zn= 0,001 %;	Sb= 0,00 01%;	Ta= 0,008 %;	W= 0,01 0%;	Pb= 0,002% %

The metallographic test - Metallographic analysis carried out was carried out in accordance with ASTM E 407-07. To reveal the microstructure of the steels, a 2% Nital solution was used, via immersion for 7 seconds. The microstructure analysis was used under an optical microscope with a bright field technique, with the purpose of studying the morphology of the microconstituents present, grain size and microhardness - HV.

For microstructural characterization, the IMAGE J® software was used for processing and digitizing the images and the Wilson Instruments Model 401 MVD® microhardness tester was used for the microhardness test with a load of 100 gf/mm².

Results and Discussion

After the 12-hour deaerated immersion test, the surfaces of the specimens were covered with corrosion products, in Figure 4a and 5a the immersed MO observe dispersed gray particles which can be attributed to residual microcrystals of sodium salts from the NACE 177-B solution. In Figure 4b of immersed MS, cracks of different shapes can be seen throughout the entire length of the corrosion layers. As expected, the pH of the NACE 177-B solution increased from ≈ 3.45 to ≈ 3.85 due to acid etching (Eq. 2).



Figure 4: SEM after 12 hour corrosion a) Immersed MO and b) Immersed MS

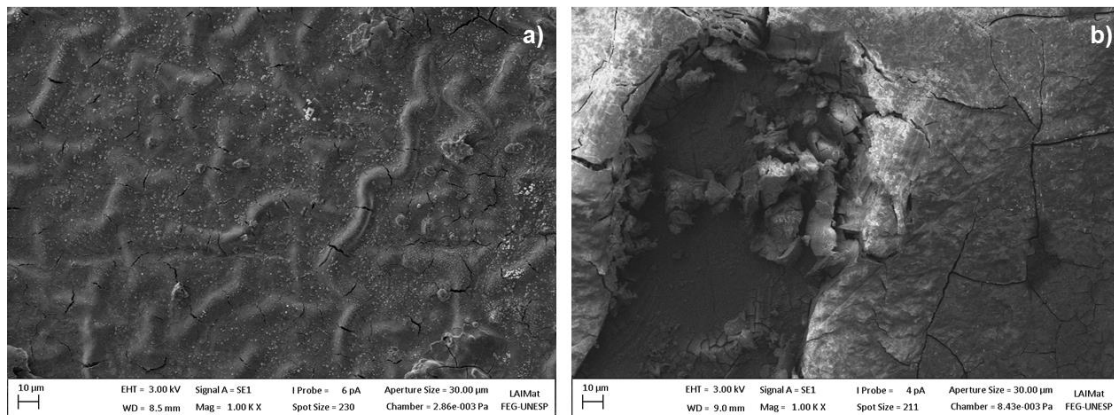


Figure 5: SEM after 12 hour corrosion a) Suspended MO and b) Suspended MS

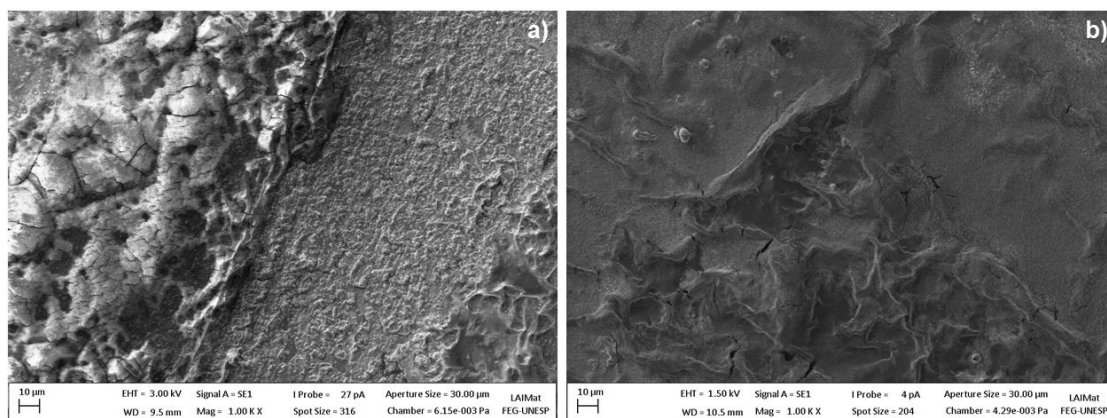
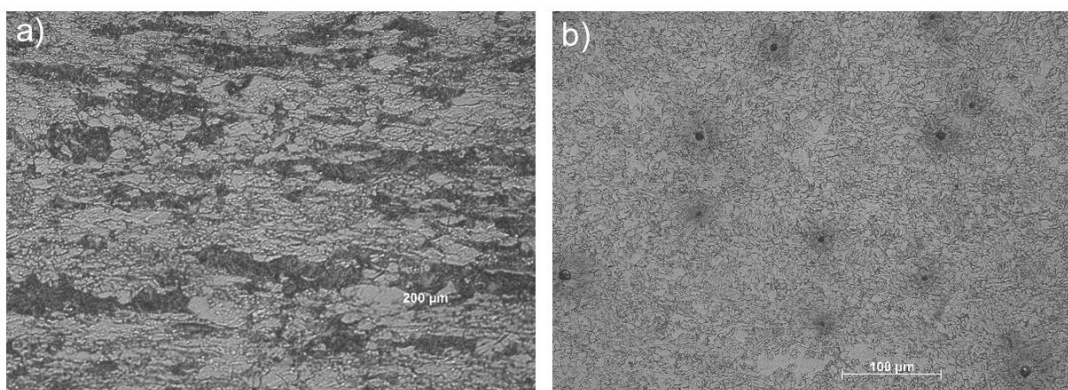


Figure 6 (a) and (b) shows the microstructure of the API 5L X70 MO and API 5L X70 MS alloy. In Figure 6 (a) the steel X70 MO presents a coarse-grained ferritic microstructure with the presence of bands (identified by the darker areas) Figure (b) observe the analysis of the surface of the steel randomly oriented (light areas) and intergranular pearlite (black spots).

The high grain refinement is due to the low carbon content and thermomechanical treatment (controlled rolling and accelerated cooling).

Figure 6: Optical micrographs of (a) X70MO and (b) X70 MS steels

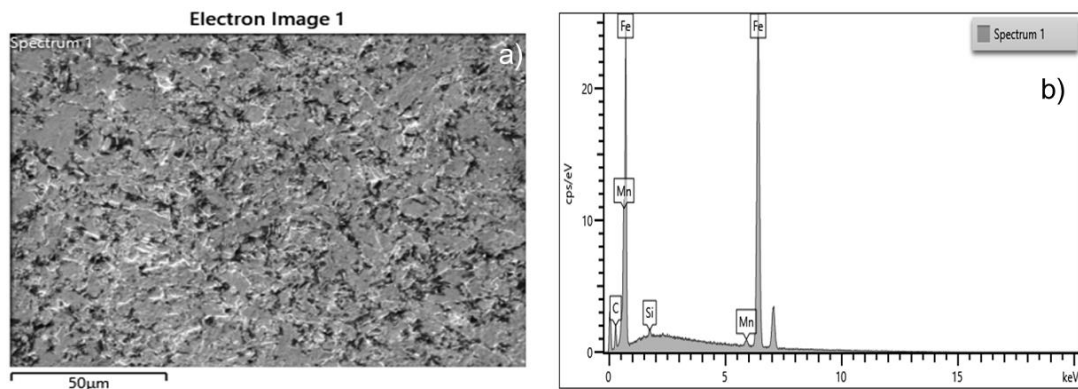


The average grain sizes and standard deviation values of microhardness in MO steel are larger than in MS steel, probably due to a more refined and homogeneous microstructure in the latter. Both steels exhibited similar average grain sizes. MO and MS steels have ferritic grain sizes of $6 \pm 3 \mu\text{m}$ and $5 \pm 2 \mu\text{m}$, respectively. The micro hardness values are similar, however the MS sample has a lower standard deviation characterized by its refined and homogeneous microstructure.

In the steel microhardness test, 20 indentations were made along the entire length, preserving the banding. The mean and standard deviation of the MO sample was $221.32\text{HV} \pm 22.63$ in the part outside the banding it was 217.04 ± 21.14 in MS $227.77\text{HV} \pm 7.60$ the corrosion resistance of specimens was When evaluating the mass loss with the reduction of the samples, MO showed greater resistance to the environment without H_2S than MS.

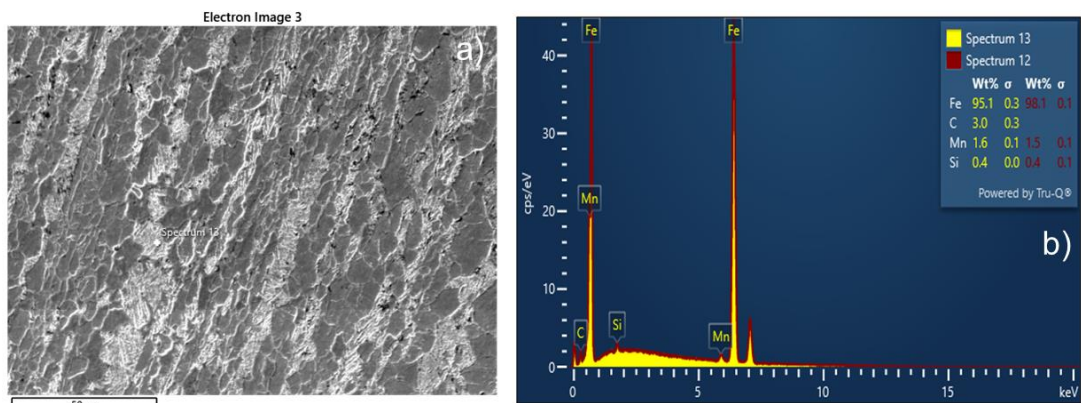
Figures 7 and 8 show the analysis of the steel carried out at 500X magnification using the scanning electron microscopy (SEM) and EDS technique. Figure 7a shows the ferritic microstructure, which showed banding (darker bands) and coarser grains, especially in the central region, which also appeared segregated. These effects can be seen in Figure 7b EDS, in which we can see a high manganese content, as reported by other authors [7 ,8].

Figure 7: a) SEM micrographs X 70 MO; b) Energy dispersive identification of elements X 70 MO steel



In Figure 8a, observe the random orientation of the light areas and the black intergranular pearlites. This refinement of the grains can be seen in the EDS (Figure 8b) which shows that it has a low carbon content, as do other authors [9,10].

Figure 8: a) SEM micrographs X 70 MS; b) Energy dispersive identification of elements X 70 MS steel



The pickling curves were similar for both MO and MS steels and both conditions (Figure 9), however the X70 MO steel was much more resistant to corrosion than X70MS as shown in Table 2 after the pickling results deaerated for 12 hour. MO steel presented greater resistance due to being able to withstand less H₂S.

Figure 9: Graph used to calculate 12- hour mass loss

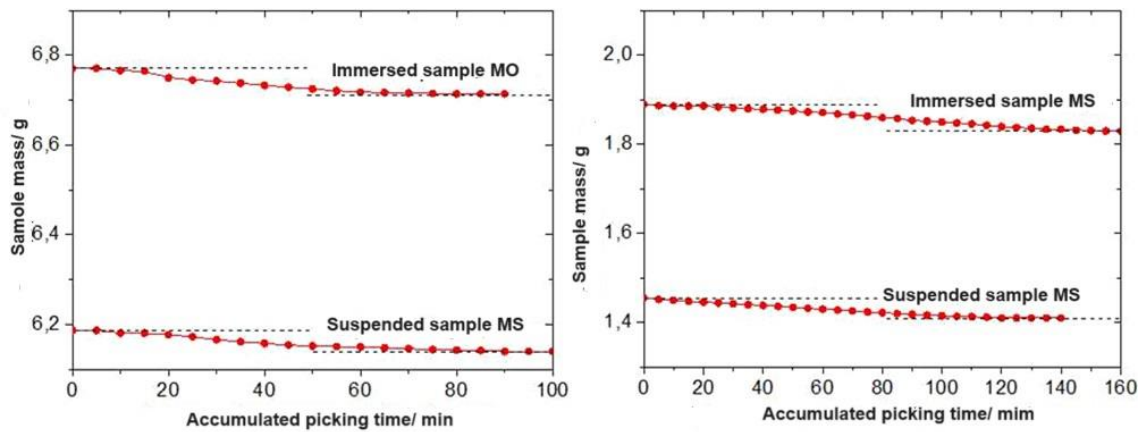


Tabela 2: Mass loss per unit area (% cm²) 12 hour of deseration

Samples	API 5L X70 MO	API 5L X70 MS
Immersed	0,084	0,27
	0,031	0,38
	0,17	0,05
	0,12	0,22
	0,35	0,018
Suspended	0,069	0,19
	0,17	0,34
	0,14	0,07
	0,22	0,16
	0,033	0,17

For the 96-hour tests, the pickling curves were similar for the two carbon steels in both conditions (Figure 10). MS steel was more resistant to corrosion than MO, as it is a steel that is more resistant to H₂S.

Figure 10: Graph used to calculate 96 hour mass loss

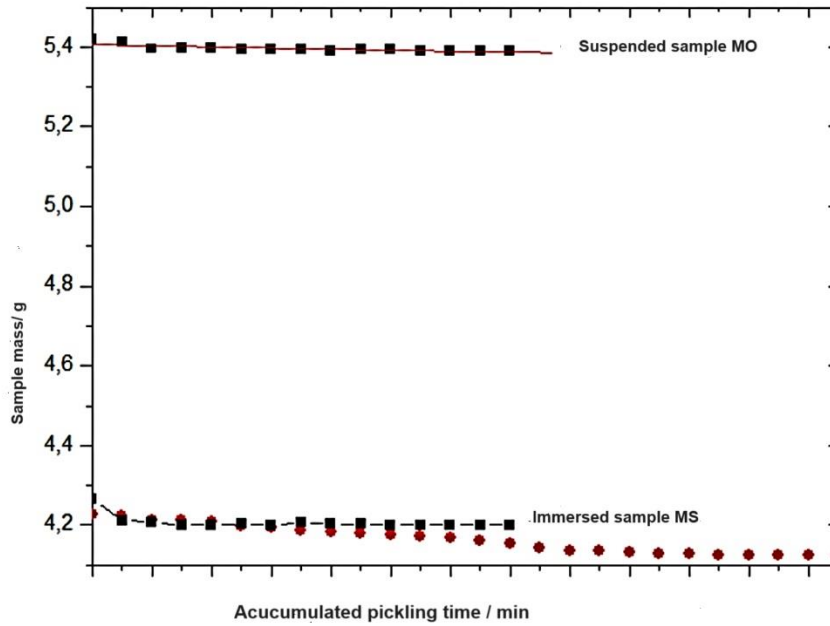


Table 3: Mass loss per unit area (% cm²) 96 hours saturated with H₂S

Samples	API 5L X70 MO	API 5L X70 MS
Immersed	0,10	0,12
	0,14	0,10
	0,16	0,14
	0,18	0,11
Suspended	0,20	0,04
	0,11	0,062
	0,07	0,09
	0,08	0,05

To characterize the corrosion products in the API 5L X-70 MO and MS steel samples, immersion and suspension tests were carried out in the test environment for 96 hours.

Figure 11: Diffractography of the corroded surfaces after 96 hours immersed in MO and MS

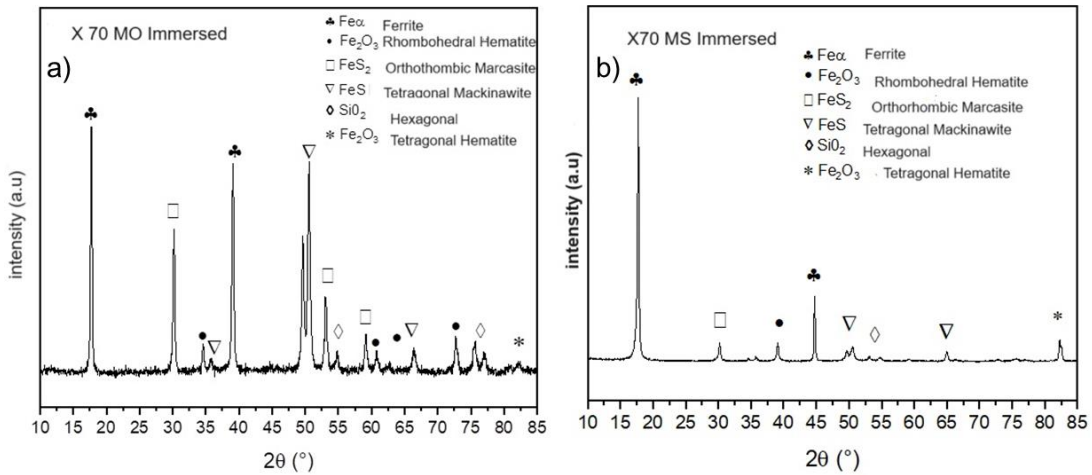


Figure 11 shows the diffraction pattern in static conditions with the characteristic that sulfides predominated over oxides. On the immersed samples, the diffractograms revealed the presence of a mixture of Tetragonal Mackinawite (FeS), Orthorhombic Marcasite (FeS $_2$) and Tetragonal Hematite (Fe $_2$ O $_3$). The presence of mackinawite (FeS) as a joint precursor was observed by the authors [10,11,12] and the growth of layers of corrosion products.

Figure 12: Diffractography of the 96-hour corroded surfaces suspended Mo and MS

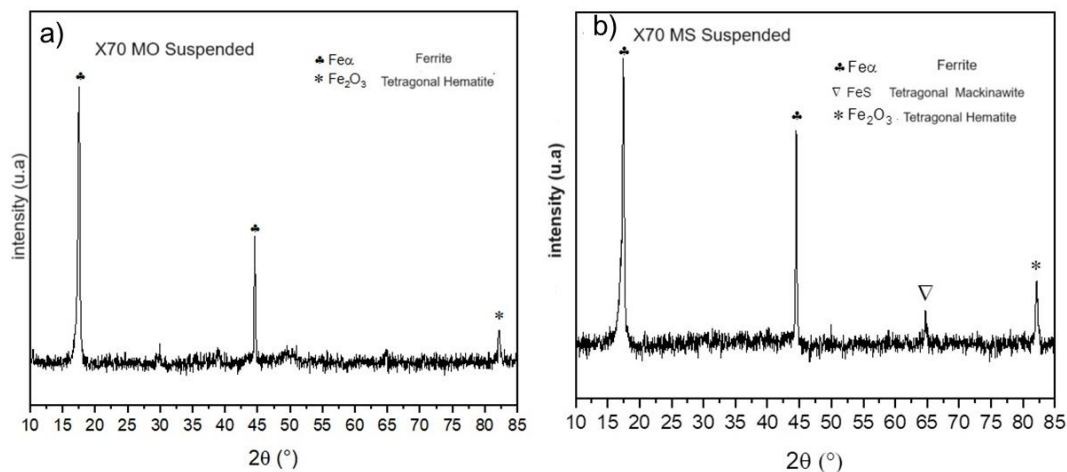


Figure 12 shows the suspended samples, Ferrite (Fe) was detected, probably because they have a thinner layer of sulfides. This layer consists of iron sulfide products, where the importance of the polymorphism of crystalline phases reported by authors is emphasized [12, 13].

Conclusions

Preliminary results revealed that X70 MO presents greater corrosion resistance than X70 MS in an H₂S-free environment. This fact may be associated with the difference in composition and/or microstructure of these steels, which has not yet been investigated.

The results indicated that X70 MO presents greater corrosion resistance than X70 MS in deaerated NACE 177-B solution, free of H₂S. This fact may be associated with the difference in composition and/or microstructure of these steels, which has not yet been investigated.

The results revealed a greater loss of mass in the immersed c-d-p of both steels, probably due to partial dissolution of the corrosion products during the tests. The X70 MS steel has a slightly higher corrosion resistance than the X70 MO under our test conditions.

Although the steels have different chemical compositions, preliminary results reveal that the composition of the corrosion products were similar. The steels immersed in the NACE 177-B solution were apparently more attacked, with Mackinawite as the predominant surface phase.

Acknowledgments

This work was supported by CAPES.

References

- [1] A. Cervantes-Tobón, M. Díaz-Cruz, J.L. González-Velázquez, J.G. Godínez-Salcedo, *Int. J. Electrochem. Sci.*, 9 (2014) 2254-2265.
- [2] ASTM E 3. Standard Guide for Preparation of Metallographic Specimens 1. , 2017.
- [3] E1382. Determining Average Grain. ASTM International, v. 97, n. Reapproved 2010, p. 1–24, 2014.
- [4] CRAIG, B., *Materials Performance* 2002, August, 2
- [5] E1382. Determining Average Grain. ASTM International, v. 97, n. Reapproved 2010, p. 1–24, 2014.
- [6] IEA - International Energy Agency; *Resources to Reserves 2013 - Oil, Gas and Coal Technologies for the Energy Markets of the Future*, OECD/IEA, Paris, 2013.
- [7] TISSOT, B.P., WELTE, D.H., *Petroleum Formation and Occurrence*, 2nd ed., Springer-Verlag: Berlin, 1984.
- [8] FIORAVANTE, I. A. et al. A review on corrosion of low carbon steels in aqueous hydrogen sulfide, **International Journal of Engineering Sciences & Research Technology**, 8(12): dec. 2019.
- [9] J.S. Smith, J.D.A. Miller, *Corrosion Journal*, 10(3) (1975) 136.
- [10] LIU, M., WANG, J., KE, W., HAN, E.H., “Corrosion behavior of X52 anti-H₂S pipeline steel exposed to high H₂S concentration solutions at 90 °C”, *J. Mater. Sci. Technol.*, v. 30, n.5, pp. 504-510, 2014.
- [11] NUNES, R. S. et al. Films Formed on Carbon Steel in Sweet Environments - A Review, **Journal Brazilian Chemical Society**, v. 30, n. 7, p. 1341-1349, 2019.
- [12] MACEDO, J.F., FIORAVANTE, I. A., NAKAZATO, R. Z., ACCIARI, H.A., CODARO, E.N., “Corrosion behavior of API 5L X70 carbon steels in hydrogen sulfide environments”, *Iranian Journal of Materials Science and Engineering*, v. 18, n. 1, March 2021.
- [13] MAHMOUD, M. A., KAMAL, M. S., GERI, B. S. B., HUSSEIN, I. A., FAHD, K., “Removal of pyrite and different types of iron sulfide scales in oil and gas wells without H₂S generation”, Paper IPTC-18279-MS of International Petroleum Technology Conference, Doha, Qatar, 2015.

[14] SMITH, S. N., BROWN, B., SUN, W., "Corrosion at higher H₂S concentrations and moderate temperatures", Paper 11081 of NACE International, Houston, Texas, 2011.

[15] SMITH, S.N., "Corrosion product analysis in oil and gas pipelines", Materials Performance, v. 44, pp. 2-4, August 2003.

[16] STUMPF, A., TOLVAJ, K., JUHÁSZ, M., "Detailed analysis of sulfides in gasoline range petroleum products with high-resolution gas chromatography-atomic emission detection using group-selective chemical treatment", Journal of Chromatography A, v. 819, n. 1-2, pp. 67-74,